ELSEVIER

Fusion Engineering and Design 28 (1995) 415–428

Fusion Engineering and Design

Radioactivity measurements of ITER materials using the TFTR D–T neutron field

Anil Kumar [a], Mohamed A. Abdou [a], Cris W. Barnes [b], H.W. Kugel [c], M.J. Loughlin [d]

[a] *School of Engineering and Applied Science, University of California at Los Angeles, Los Angeles, CA 90095, USA*
[b] *Los Alamos National Laboratory, Los Alamos, NM 87545, USA*
[c] *Princeton Plasma Physics Laboratory, Princeton University, Princeton, NJ 08543, USA*
[d] *JET Joint Undertaking, Abingdon, Oxfordshire OX14 3EA, UK*

Abstract

The availability of high D–T fusion neutron yields at TFTR has provided a useful opportunity to measure directly D–T neutron-induced radioactivity in a realistic tokamak fusion reactor environment for materials of vital interest to ITER. These measurements are valuable for characterizing radioactivity in various ITER candidate materials, for validating complex neutron transport calculations, and for meeting fusion reactor licensing requirements. The radioactivity measurements at TFTR involve potential ITER materials including stainless steel 316, vanadium, titanium, chromium, silicon, iron, cobalt, nickel, molybdenum, aluminum, copper, zinc, zirconium, niobium, and tungsten. Small samples of these materials were irradiated close to the plasma and just outside the vacuum vessel wall of TFTR, locations of different neutron energy spectra. Saturation activities for both threshold and capture reactions were measured. Data from dosimetric reactions have been used to obtain preliminary neutron energy spectra. Spectra from the first wall were compared with calculations from ITER and with measurements from accelerator-based tests.

1. Introduction

The licensing of high power fusion reactors will require certification of calculations of induced radioactivity. A database of measured radioactivity in environments with prototypical neutron spectra is crucial for this purpose. A concerted beginning was made by an extensive experimental program using accelerator-based neutron sources on induced radioactivity measurements in small samples of fusion reactor relevance in the framework of a USDOE–JAERI collaboration [1–5]. The analysis of those meaurements with various radioactivity codes and activation libraries revealed relatively large sources of discrepancies in calculations. These discrepancies were related to many contributing factors, including decay γ half-lives, γ yields, neutron energy spectra, and activation cross-sections.

Engineering design activities of the International Thermonuclear Experimental Reactor (ITER) are already underway. Radioactivity calculations for the ITER neutron environment may suffer even larger discrepancies between calculations and measurements than did the accelerator-based experiments with their inherently superior neutron spectrum characterization. Conducting comparison experiments on existing tokamaks should significantly improve extrapolations to ITER. The Tokamak Fusion Test Reactor (TFTR) has been one of the front-line experimental devices on tokamak-

Elsevier Science S.A.
SSDI 0920-3796(94)00375-0

based magnetic fusion research. There were previous attempts to characterize the neutron energy spectra emitted from the device using a point D–T neutron generator[6,7]. However, the errors on these experimental measurements were quite large owing to poor counting statistics. Later, an extensive experimental campaign was conducted with various film badges and dosimeters to map the biological doses from the test cell walls out to the site boundary during high power D–D discharges [8–10]. The D–T campaign of TFTR initiated in November 1993 provided an excellent opportunity to carry out induced radioactivity measurements [11]. Measurements were made from samples of aluminum, silicon, titanium, vanadium, chromium, iron, cobalt, nickel, copper, zinc, zirconium, niobiun, molybdenum, indium, tungsten, and gold at various locations around TFTR. In this paper, we report on measurements made close to the plasma and vacuum vessel. A companion paper will discuss measurements on samples irradiated on the inner walls of the TFTR test cell [12].

2. Experiments

Samples were exposed to the TFTR neutron field using the pneumatic transfer system of the neutron activation diagnostic [13–17]. They were irradiated for one to several plasma discharges, with the neutrons primarily emitted during the approximately 1 s duration of the neural beam injection, and the discharges occurring about 10–20 min apart. A typical foil used for lower intensity D–D or D–T discharges measures 1 mm thickness (except gold foils were 0.025 mm thick) by 18 mm diameter (except stainless steel 316 foils have a diameter of 10 mm) and has very high purity. For high yield D–T discharges the foils were broken into smaller pieces to limit the total dose rate just after its extraction. After irradiation, all the foils were taken out from a single capsule and different capsules (some containing more than one foil) were prepared for counting. Three different irradiation ends (IEs) or terminal locations of the transport system were used. Foils irradiated in the re-entrant location IE 8 are at a major radius of 2.58 m and 1.039 m above the midplane [16]. Re-entrant end IE 8 extends in from a racetrack flange on top of the vacuum vessel. It sees the hardest neutron energy spectrum with its proximity to the plasma (it represents the only irradiation end that falls within the nuclear boundary). IE 4 and IE 3 are located outside the vaccum vessel in the midplane of two different toroidal "bays" between TF coils. IE 4 is located 407.6 cm in major radius, and 7.6 cm below the actual midplane in bay F [15]. IE 3 is at a similar position somewhat above the midplane in bay B. Two high purity germanium (HPGe) detectors were used for γ spectroscopy of the irradiated foils after appropriate cooling times. Absolute efficiencies for both detectors have been determined using NIST-traceable standard sources [15,16].

For our studies several particular sets of measurements were done:

- A single capsule containing 14 foils (Al, Ti, V, Fe, Co, Ni, stainless steel (SS) 316, Cu, Zn, Zr, Nb, Mo, In, and W) was irradiated in IE 8 during four trace tritium discharges on November 22, 1993. The accumulated D–T and D–D neutron yields were 5.6×10^{15} and 5.0×10^{16} respectively, yielding 10% of the total source neutron emission being contributed by D–T neutrons alone. The radioactive products and γ peaks of interest were the same as those reported earlier in Refs. 4 and 3. The cooling times ranges from 1 h 41 min to 15 h 40 min. The counting times ranged from 10 min to 3 h 15 min.
- Pairs of identical capsules were irradiated in single D–D supershots on February 24 and 25, 1994. Two identical capsules (Fe, Ni, Co, Cr, Mo, Nb, Al, and Au) were irradiated in IE 8 and IE 4 with D–T and D–D neutron yields of 1.4×10^{15} and 1.25×10^{16} respectively, for a D–T contribution again amounting to 10% of the total yield (this amount of D–T neutron yield coming from tritium recycling from the wall). Cooling times ranged from 1 h 36 min to 1 day 16 h. Two identical capsules (Al, V, and W) were irradiated in IE 8 and IE 3 with D–T and D–D neutron yields of 8.1×10^{14} and 8.2×10^{15} respectively, for a D–T contribution amounting to 9.0% of the total yield. A second pair (Al, Ti, Zr, and Au) in IE 8 and IE 3 had D–T and D–D neutron yields of 1.2×10^{15} and 1.26×10^{16} respectively, for a D–T contribution amounting to 8.7% of the total yield. Cooling times ranged from 1 h 32 min to 5 h 27 min.
- Eight sets of two identical capsules were irradiated in IE 8 and IE 3 on February 28 and March 1, 1994, during different D–T supershots. An aluminum foil was in all the irradiated capsules. The other irradiated foils included Ti, V, Cr, Fe, Co, Ni, Cu, Zr, Nb, Mo, W, and Au. D–T neutron yields per discharge varied from 6.4×10^{17} to 2.2×10^{17}; D–D neutron yields were unmeasurable in these conditions but expected to be about 40 times lower. The cooling times ranges from 12 min 31 s to 23 days 23 h.

In addition to these specific measurements, many other extensive measurements using aluminum, silicon, and indium foils have been made routinely.

3. Experimental analysis

The spectra from the HPGe detector were analyzed by an analysis package on an IBM-XT [13,15]. Decay γ yields and half lives were adopted from a table of radioactive isotopes [18]; isotopic fractions were adopted from the older table of isotopes [19]. When counting with more than one foil in a single capsule, the calculation of accurate γ self-shielding for each γ peak was very important. A Monte Carlo program was used to obtain net correction factors that take into account changes in absolute detector efficiency with distance as well as γ self-shielding for all γ rays emitted by each foil in a counted capsule. The largest number of foils in a counted capsule was five. Diameter, thickness, density of each foil, relative foil arrangement, capsule–detector distance, and detector diameter were among the parameters needed to be specified for this program. Energy dependent γ attenuation coefficients were taken from Ref. [20]. Saturation activities for all observed γ peaks from each radioactive isotope were intercompared and found to agree within experimental error.

A number of parameters affect experimental error estimation. These include counting statistics, the half-life of γ emitter, accuracy of the HPGe detector efficiency, the cooling and counting times, the activation cross-section, and various nuclear coefficients. Sum-peak corrections also add to the error. It is impossible to give a single figure for even one sample material; however, for most of the experimental measurements, the accuracy of the saturation activity is between 6% and about 14% [17].

4. Discussion of processed data

As a large number of isotopic activiites of importance to ITER were measured close to the TFTR device in different locations, there are a number of ways one can discuss the measured data. In what follows, we present a succinct discussion on various aspects of interest to both ITER and further experimental efforts at TFTR.

4.1. Overview of saturation activities

Tables 1 and 2 and Fig. 1 give the various dosimetric reaction products, and the saturation activity (activated nuclei per source neutron per target nuclei) for the materials irradiated at TFTR and discussed in this paper. All threshold reactions' activities were normalized to one D–T source neutron, whereas all capture reactions' activities were normalized to a TFTR source neutron (D–T + D–D). The reactions and their products include the following: (1) ^{197}Au(n,γ)^{198}Au, (2) ^{59}Co(n,γ)$^{60m+g}$Co, (3) ^{58}Ni(n,p)$^{58m+g}$Co, (4) ^{54}Fe(n,p)^{54}Mn, (5) ^{46}Ti(n,p)^{46}Sc + ^{47}Ti(n,n'p or d)^{46}Sc + ^{48}Ti(n,n'd or t)^{46}Sc, (6) ^{47}Ti(n,p)^{47}Sc + ^{48}Ti(n,n'p or d)^{47}Sc + ^{49}Ti(n,n'd or t)^{47}Sc, (7) ^{48}Ti(n,p)^{48}Sc + ^{49}Ti(n,n'p or d)^{48}Sc + ^{50}Ti(n,n'd or t)^{48}Sc, (8) ^{27}Al(n,α)^{24}Na, (9) ^{56}Fe(n,p)^{56}Mn, (10) ^{59}Co(n,α)^{56}Mn, (11) ^{93}Nb(n,2n)^{92m}Nb, (12) ^{59}Co(n,2n)$^{58m+g}$Co, (13) ^{90}Zr(n,2n)$^{89m+g}$Zr, and (14) ^{58}Ni(n,2n)^{57}Ni. Only a single target atom is to be understood as assigned to each of these twelve radioactive products and they are respectively as follows: (1) ^{197}Au, (2) ^{59}Co, (3) ^{58}Ni, (4) ^{54}Fe, (5) ^{46}Ti, (6) ^{47}Ti, (7) ^{48}Ti, (8) ^{27}Al, (9) ^{56}Fe, (10) ^{59}Co, (11) ^{93}Nb, (12) ^{59}Co, (13) ^{90}Zr and (14) ^{58}Ni. These reactions on the abscissa, the horizontal axis, of Fig. 1 are arranged approximately in the order of increasing effective neutron energy threshold, with the first two reactions being capture reactions. Note that each reaction is assigned a number, e.g. ^{197}Au(n,γ)^{198}Au is assigned value of 1 on horizontal axis of Fig. 1. Where available, data for all three IEs, i.e. 8, 3, and 4, is shown. The largest saturation activities occur for the two capture reactions, i.e. ^{197}Au(n,γ)^{198}Au, and ^{59}Co(n,γ)$^{60m-g}$Co. These clearly signal the strong presence of thermal neutrons at the low end of the neutron energy spectrum. As for threshold reactions, the saturation activity varies from 5×10^{-33} to 1×10^{-30} per target nucleus.

Figs. 2 and 3 show saturation activity per source neutron per sample atom for various materials of relevance to ITER, for other threshold (Fig. 2) as well as capture (Fig. 3) reactions. In these prototypical plots, we have primarily included those products which have earlier been subject of large discrepancies between calculations and measurements [1–4]. Each of these measured saturation activities have been normalized to all isotopes of a sample atom, including those that do not participate in reaction of interest. ^{69m}Zn is included in both the figures as there are two competing reactions: ^{70}Zn(n,2n)^{60m}Zn and ^{68}Zn(n,γ)^{69m}Zn. Even though ^{90}Mo is included only in Fig. 3, both a threshold and a capture reaction produce it: ^{100}Mo(n,2n)^{99}Mo, and ^{98}Mo(n,γ)^{99}Mo. Similarly, ^{51}Cr has two contributing reactions, i.e. ^{52}Cr(n,2n)^{51}Cr, and ^{50}Cr(n,γ)^{51}Cr. From both the figures, it is clear that cobalt has largest saturation activities, for both threshold reaction, ^{59}Co(n,2n)$^{58m+g}$Co, and capture reaction, ^{59}Co(n,γ)$^{60m+g}$Co. Lowest threshold reaction activity comes from ^{51}V(n,α)^{48}Sc, primary component of vanadium–chromium–titanium alloys being considered actively as

Table 1
Observed γ-emitting isotopes of materials irradiated at TFTR

Material (foil)	Product and half-life	Material (foil)	Product and half-life
Al	2.24 min ^{28}Al, 9.46 min ^{27}Mg, 15 h ^{24}Na	Zn	2.52 h ^{65}Ni, 12.7 h ^{64}Cu, 13.8 h ^{69m}Zn, 2.58 day ^{67}Co, 244.1 day ^{65}Zn
Si	2.24 m ^{28}Al, 6.56 m ^{29}Al, 9.46 min ^{27}Mg	Zr	49.7 min ^{91m}Y, 72 min ^{97}Nb, 2.8 h ^{87m}Sr, 3.19 h ^{90m}Y, 9.52 h ^{91}Sr, 16.9 h ^{97}Zr, 78.4 h ^{89}Zr, 64 day ^{96}Zr
Ti	3.93 h ^{44}Sc, 43.7 h ^{48}Sc, 3.34 day ^{47}Sc, 4.54 day ^{47}Ca, 83.8 day ^{46}Sc	Nb	3.19 h ^{90m}Y, 10.2 day ^{92m}Nb
V	3.75 min ^{52}V, 5.76 min ^{51}Ti, 43.7 h ^{48}Sc	Mo	6.85 h ^{93m}Mo, 23.4 h ^{96}Nb, 66 h ^{99}Mo, 78.4 h ^{89}Zr, 10.2 day ^{92m}Nb, 35 day ^{95}Nb
Cr	41.9 min ^{49}Cr, 27.7 day ^{51}Cr	SS 316	2.58 h ^{56}Mn, 36 h ^{57}Ni 66 h ^{99}Mo, 44.6 day ^{59}Fe
Fe	2.58 h ^{56}Mn, 27.7 day ^{51}Cr, 312.2 day ^{54}Mn	In	54.2 min ^{116m}In, 4.49 h ^{115m}In
Co	2.58 h ^{56}Mn, 44.6 day ^{59}Fe, 70.8 day ^{58}Co, 5.3 year ^{60}Co	W	23.9 h ^{187}W
Ni	2.52 h ^{65}Ni, 36 h ^{57}Ni, 70.8 day ^{58}Co, 271 day ^{57}Co	Au	9.7 h ^{196m2}Au, 2.69 day ^{198}Au, 6.18 day ^{196}Au
Cu	12.7 h ^{64}Cu		

Table 2
Saturation activities for titanium, iron, nickel, cobalt, and molybdenum (DT discharges at TFTR)

Material (foil)	Product	Saturation activity [a]		Material (foil)	Product	Saturation activity [a]	
		IE 8	IE 3			IE 8	IE 3
Ti	^{44}Sc	3.27×10^{-35}		Ni	^{65}Ni		2.06×10^{-33}
	^{48}Sc	5.40×10^{-32}	7.97×10^{-33}		^{57}Ni	2.07×10^{-32}	2.62×10^{-33}
	^{47}Sc	2.08×10^{-32}	3.26×10^{-33}		^{58}Co	4.324×10^{-31}	7.15×10^{-32}
	^{47}Ca	3.80×10^{-34}	–		^{57}Co	1.22×10^{-30}	1.74×10^{-31}
	^{46}Sc	3.13×10^{-32}	–				
Fe	^{56}Mn	1.36×10^{-31}	2.48×10^{-32}	Mo	^{93m}Mo	3.53×10^{-34}	–
	^{51}Cr	6.62×10^{-33}	–		^{96}Nb	4.05×10^{-33}	5.07×10^{-34}
	^{54}Mn	3.42×10^{-32}	1.89×10^{-32}		^{99}Mo	3.53×10^{-31}	1.49×10^{-31}
					^{89}Zr	4.89×10^{-33}	–
Co	^{56}Mn	3.40×10^{-32}	6.14×10^{-33}		^{92m}Nb	1.59×10^{-32}	4.19×10^{-33}
	^{59}Fe	7.23×10^{-32}	1.17×10^{-32}		^{95}Nb	8.32×10^{-33}	–
	^{58}Co	8.59×10^{-31}	1.19×10^{-31}				
	^{60}Co	3.59×10^{-30}	4.36×10^{-30}	W	^{187}W	2.95×10^{-30}	3.07×10^{-30}

[a] Each activity is normalized to one source neutron and one material atom. One standard deviation of mean experimental error is about 10% on all saturation activities.

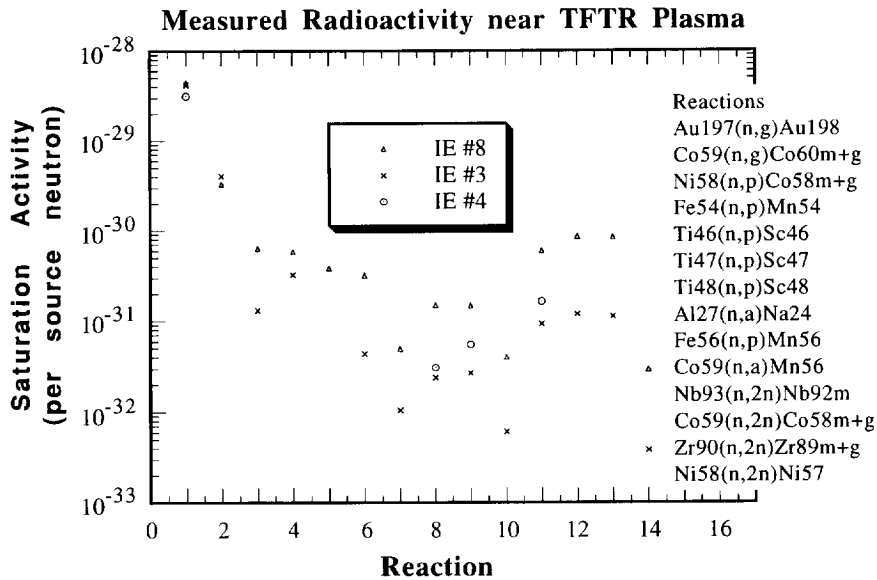

Fig. 1. Measured saturation activity per source neutron per target atom near plasma for dosimetric reactions for IEs 8, 3, and 4.

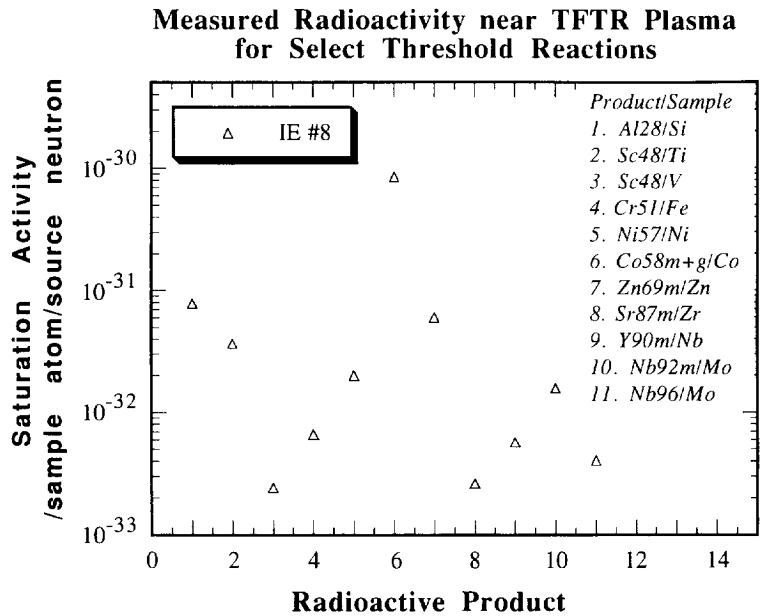

Fig. 2. Measured saturation activity per source neutron per target atom near plasma for select threshold reactions in various materials.

a low activation structural material for ITER. Lowest capture reaction activity pertains to $^{64}Ni(n,\gamma)^{65}Ni$, being at least one to two orders of magnitude lower than others (see Fig. 3). This is primarily due to the very low abundance of ^{64}Ni in natural nickel, being just 0.91%.

Comparing the saturation activities for threshold and capture reaction products, one can notice that the largest capture radioactivity, i.e. $^{60m+g}Co$, is almost an order of magnitude larger than the largest threshold radioactivity, i.e. $^{58m+g}Co$.

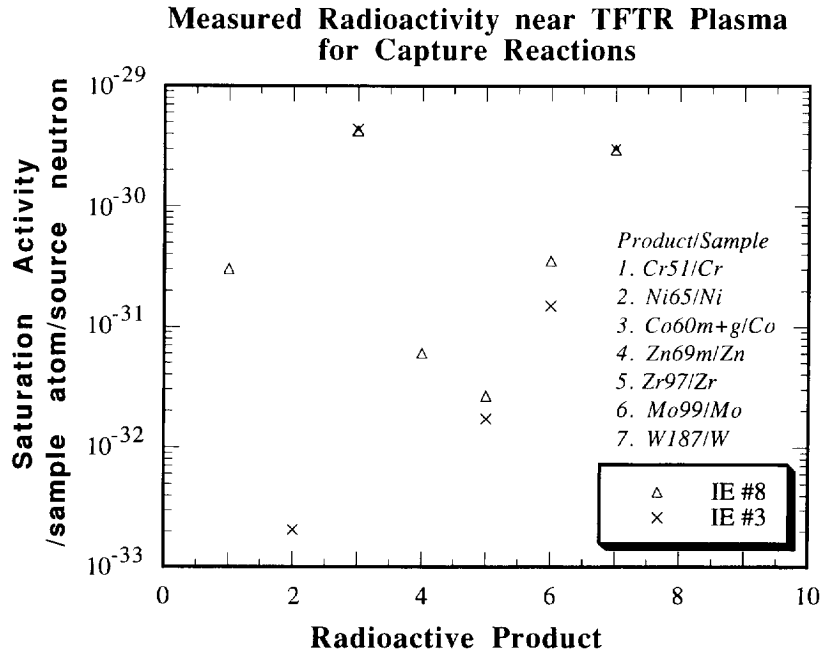

Fig. 3. Measured saturation activity per source neutron per target atom near plasma for capture reactions in various materials.

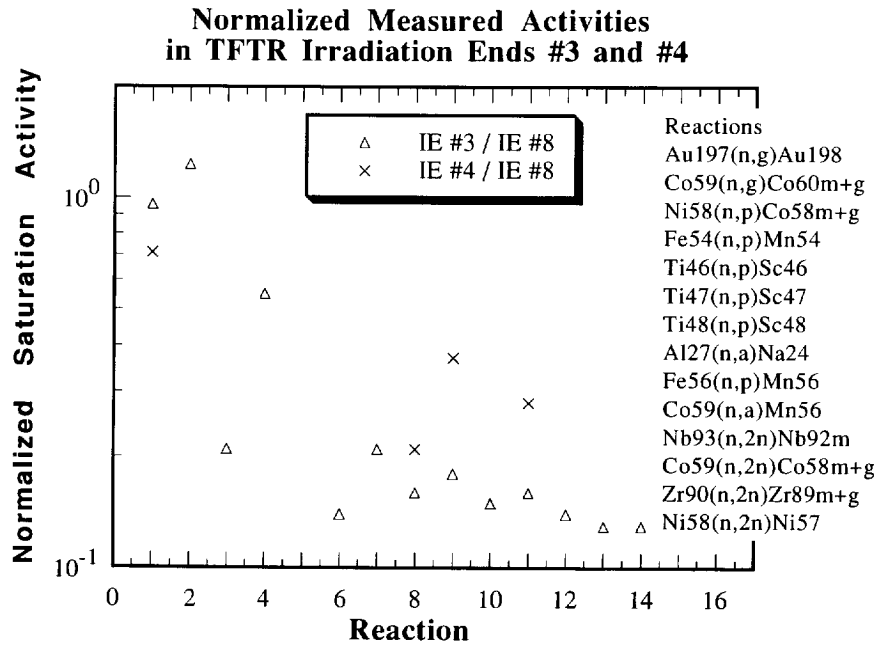

Fig. 4. Measured saturation activities for samples irradiated at IEs 3 and 4 normalized to TFTR those for IE 8, for dosimetric reactions.

From Figs. 1 and 3, one can observe that the measured saturation activities reflect a dependence on the IE. Most often, IE 8 (inside the vessel) has the largest value of the three ends and represents the "hardest" or least scattered spectrum. In Fig. 4, we present saturation activities for IEs 3 and 4 after normalizing with respect to the values at IE 8. All the dosimetric products covered in Fig. 1 are included. The spectrum for IE

3 is significantly softer than for IE 4. The measured activity for capture reaction product ^{198}Au is significantly larger (about 25%) for IE 3 as compared with that for IE 4. On the contrary, the measured saturation activities for threshold reaction products ^{24}Na and ^{56}Mn in IE 4 are significantly larger (almost by as much as 30%–50%) than those for IE 3.

MCNP [21] modeling of IE 8 has been performed to use saturation activities for a number of dosimetric products to determine neutron yields on TFTR [17]. For all dosimetric threshold reactions considered the yields agree to within $\pm 7\%$ accuracy of the TFTR systems [16]. This comparison ensures confidence in the quality of the processed data from the neutron activation system. However, it does not ensure that accurate modeling is possible for the capture reactions in IE 8 or for all investigations for both IE 3 and IE 4. Further analysis is necessary to investigate the status of prediction capability for the bulk of the measured data.

4.2. Material-wise presentation of measured saturation activities

Extensive data have been obtained for practically all materials of interest to ITER. This database could be used variously by different users. For example, it could be used to test and adjust three-dimensional models of TFTR. Engineering design studies and the regulatory licensing required for ITER can make use of these results as a reference for preliminary validation of activation calculations for the first wall. In what follows, we will give additional summary information not listed in Table 2 on the status on saturation activities measured in various materials, while graphical results will be presented for only a few of the materials. Once saturation activities are known, it is straightforward to obtain decay–γ and other source terms required for the decay–heat and/or biological dose calculations.

Aluminum

2.24 min (half-life) ^{28}Al, 9.46 min ^{27}Mg, and 15 h ^{24}Na activities were measured. Together with silicon, aluminum activation has been done routinely at TFTR to monitor D–T neutrons.

Silicon

Activities were measured for 2.24 min (half-life) ^{28}Al, 6.56 min ^{29}Al, and 9.46 min ^{27}Mg. Silicon has been used extensively at TFTR for D–T neutron monitoring because of its quite short half life.

Titanium

Most frequently observed products include 3.93 h (half-life) ^{44}Sc, 43.7 h ^{48}Sc, 3.34 day ^{47}Sc, 4.54 day ^{47}Ca, and 83.8 day ^{46}Sc. In one of the very first measurements, 5.8 min ^{51}Ti was also observed. Fig. 5 shows the saturation activity per sample atom per TFTR source neutron for IEs 8 and 3. It turns out that, for both of the locations, ^{48}Sc, ^{47}Sc, and ^{46}Sc dominate. Systematically, the measurements for IE 3 are significantly lower.

Vanadium

3.75 min ^{52}V, 5.76 min ^{51}Ti, and 43.7 h ^{48}Sc were observed.

Chromium

41.9 min ^{49}Cr and 27.7 day ^{51}Cr saturation activities were measured in a number of chromium samples.

Iron

2.6 h (half-life) ^{56}Mn, 27.7 day ^{51}Cr, and 312.2 day ^{54}Mn were observed. Fig. 6 shows the measured activities for IEs 8 and 3. ^{56}Mn activity dominates. Also, this activity is most sensitive to the spectrum as one sees a large divergence for the two ends (see Fig. 6).

Cobalt

2.6 h ^{56}Mn, 44.6 day ^{59}Fe, 70.8 day ^{58}Co, and 5.3 year ^{60}Co were detected almost routinely in most of the irradiations. Fig. 7 is a graphic presentation of the saturation activities for IE 8 and 3. One can observe the dominance of ^{60}Co and ^{58}Co. Also, relative insensitivity of ^{60}Co to neutron energy spectrum comes out very clearly.

Nickel

2.52 h ^{65}Ni, 36 h ^{57}Ni, 70.8 day ^{58}Co, and 271 day ^{57}Co activities were measured. Again, large divergence between IEs 8 and 3 was seen for ^{57}Ni, ^{58}Co, and ^{57}Co.

Copper

12.7 h ^{64}Cu activity was observed.

Zinc

2.52 h ^{65}Ni, 12.7 h ^{64}Cu, 13.8 h ^{69m}Zn, 2.58 day ^{67}Cu, and 244.1 day ^{65}Zn activities were observed.

Zirconium

Measured activities included 49.7 min (half-life) ^{91m}Y, 72 min ^{97}Nb, 2.8 h ^{87m}Sr, 3.19 h ^{90m}Y, 9.52 h ^{91}Sr, 16.9 h ^{97}Zr, 78.4 h ^{89}Zr, and 64 day ^{95}Zr. ^{89}Zr saturation activity dominated, followed by ^{95}Zr and ^{97}Zr. Large divergences for the two IEs were observed for

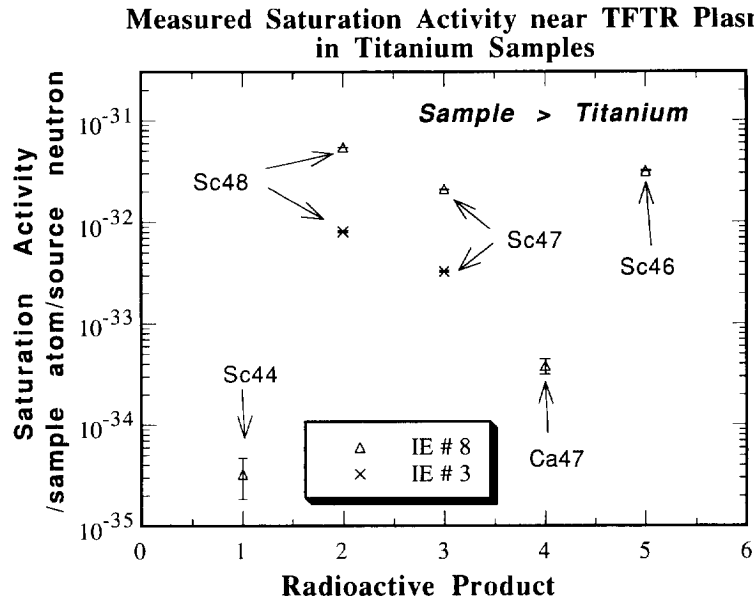

Fig. 5. Titanium: measured saturation activity per TFTR source neutron per sample atom near plasma for all its observed radioactive products.

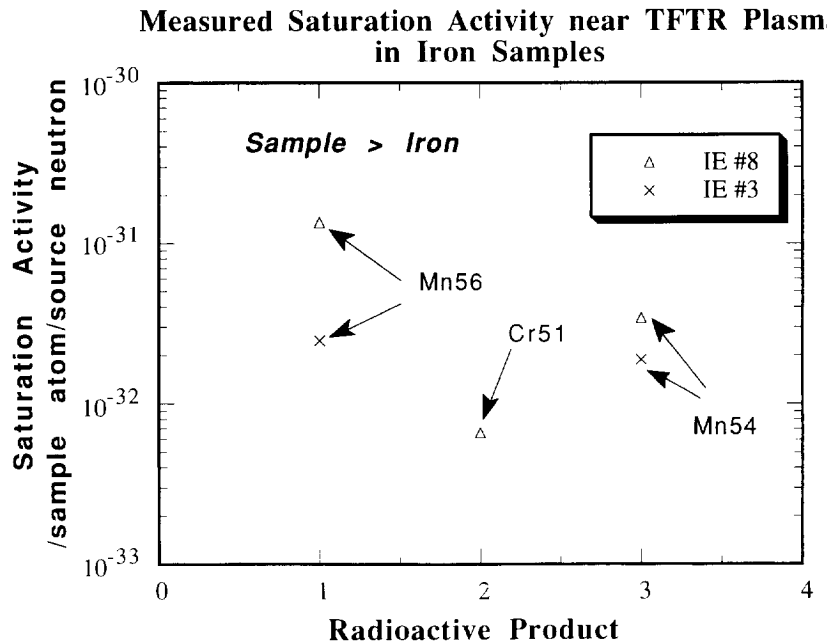

Fig. 6. Iron: measured saturation activity per source neutron per sample atom near plasma for all its observed radioactive products.

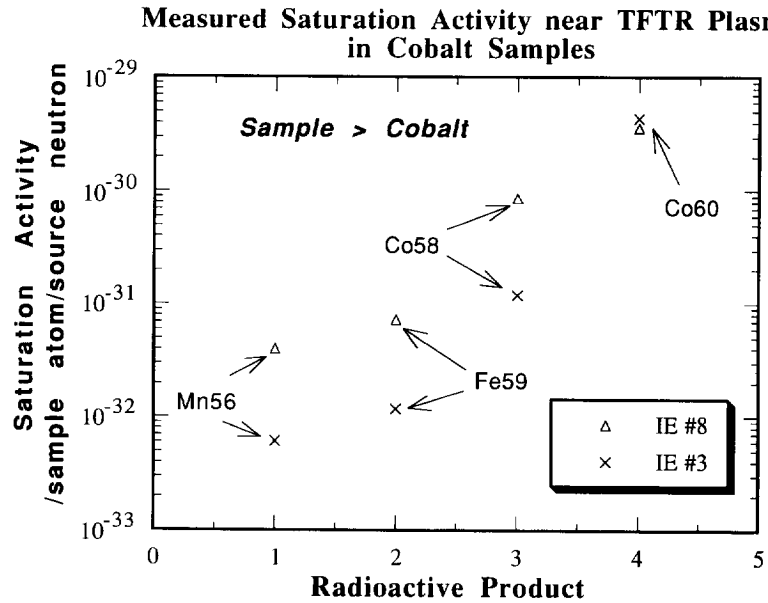

Fig. 7. Cobalt: measured saturation activity per source neutron per sample atom near plasma for all its observed radioactive products.

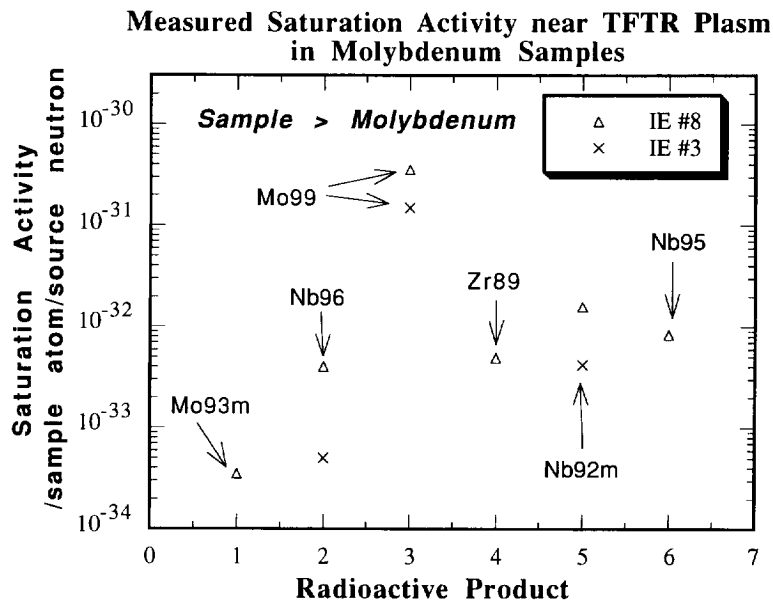

Fig. 8. Molybdenum: measured saturation activity per source neutron per sample atom near plasma for all its observed radioactive products.

^{89}Zr, ^{90m}Y, ^{87m}Sr, ^{91m}Y. ^{97}Zr, ^{91}Sr, and ^{97}Nb have much less divergences. ^{95}Zr appears to be an intermediate case. This might be due to this product receiving contributions from a contrasting set of reactions, i.e. a threshold, ^{96}Zr(n,2n)^{95}Zr, and a capture, ^{94}Zr(n,γ)^{95}Zr reaction.

Niobium

Both 3.19 h ^{90m}Y and 10.15 day ^{92m}Nb saturation activities were measured.

Molybdenum

Fig. 8 graphically displays the activities measured for

IE 8 and 3. The observed products include 6.85 h ^{93m}Mo, 23.4 h ^{96}Nb, 66 h ^{99}Mo, 78.4 h ^{89}Zr, 10.15 day ^{92m}Nb, and 34.97 day ^{95}Nb. Again, relatively large divergences for the two ends were observed whenever a threshold reaction generated the radioactivity.

Stainless steel 316

The observed activities include 2.6 h ^{56}Mn, 36 h ^{57}Ni, 66 h ^{99}Mo, and 44.6 day ^{59}Fe.

Indium

54.2 min ^{116m}In and 4.49 h ^{115m}In activities were measured.

Tungsten

23.9 h ^{187}W was observed in all irradiations.

Gold

9.7 h ^{196m_2}Au, 2.69 day ^{198}Au, and 6.18 day ^{196}Au saturation activities were measured.

Water

Preliminary measurements on water-filled microcentrifuge tubes have been initiated. These measurements will be continued, associated studies of possible systematic uncertainties will be performed, and the results will be presented at a later time. Measurement of 7.13 s, ^{16}O(n,p)^{16}N activity has assumed importance as one of the current design options of ITER deploys water as a coolant. Some designers predict that the transport of radioactive water (carrying ^{16}N) close to the superconducting toroidal magnets in this design would lead to excessive heating in the magnet and will necessitate significant changes in the current design.

5. Spectral information

There is a noticeable dependence of capture reaction products on the D–T neutron fraction. Fig. 9 shows saturation activities for five capture reactions, e.g.,

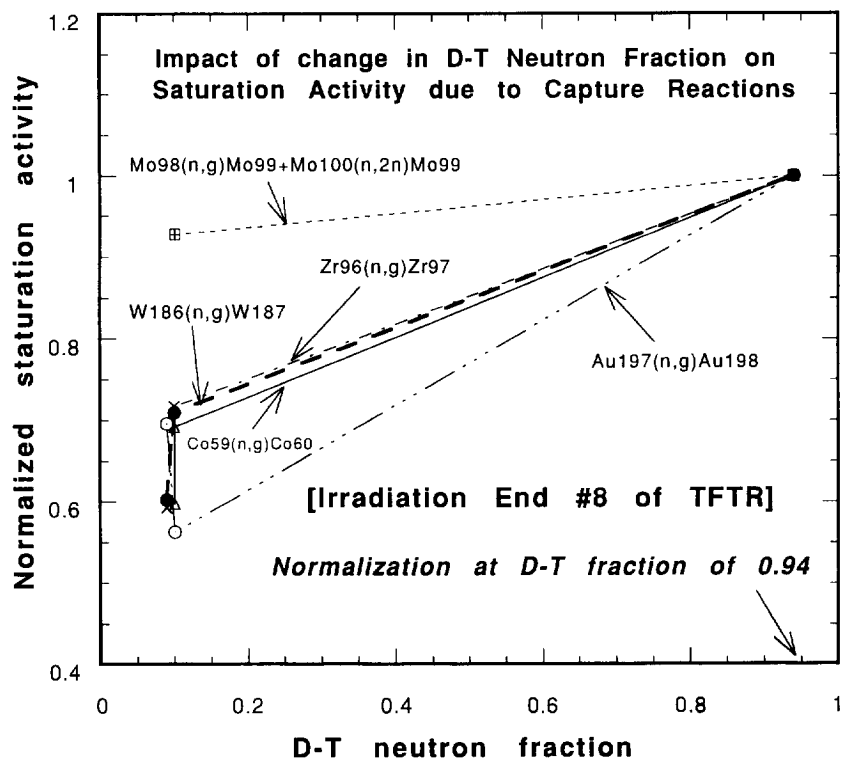

Fig. 9. Impact of change in D–T neutron fraction of a TFTR source neutron on saturation activity due to capture reactions at IE 8 of TFTR. Results for five radioactive products, i.e. ^{60}Co (from Co), ^{97}Zr (from Zr), ^{90}Mo (from Mo), ^{187}W (from W), and ^{198}Au (from Au) are shown.

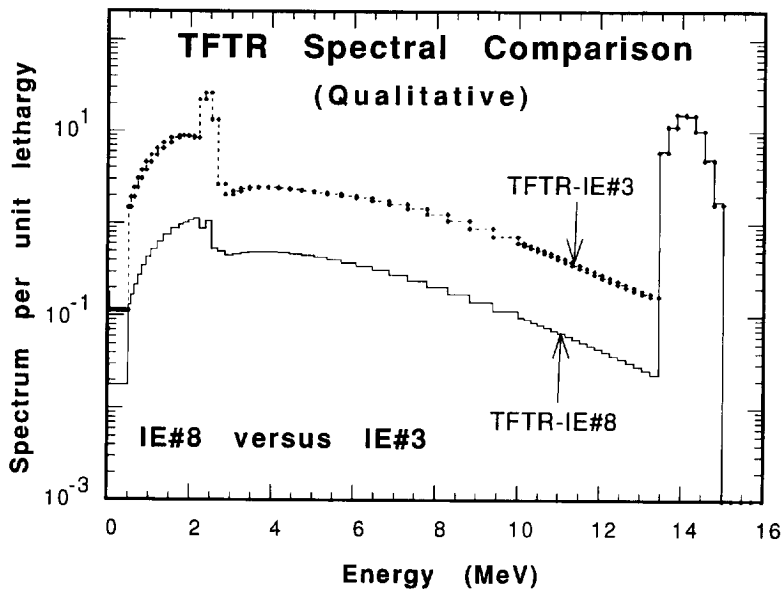

Fig. 10. Qualitative comparison of unfolded spectra for TFTR IEs 8 and 3, near plasma.

$^{59}Co(n,\gamma)^{60}Co^{g+m}$, $^{96}Zr(n,\gamma)^{97}Zr$, ^{99}Mo from Mo, $^{186}W(n,\gamma)^{187}W$, and $^{197}Au(n,\gamma)^{198}Au$, as a function of D–T neutron fraction or IE 8. The activities were normalized to their values for D–T neutron fraction of about 0.94 (February 28, 1994, irradiation). Up to about 50% change in saturation activity is seen as the D–T neutron fraction is varied from 10% to about 94%. ^{99}Mo shows a much smaller change. We infer that the "worth" of a D–T neutron to the low end of neutron energy spectrum is larger than that of a D–D neutron. A similar trend has also been observed for measurements made on inner walls of TFTR test cell [12].

The availability of measured, dosimetric, saturation activities can allow unfolding of the neutron energy spectrum for various IEs. The D–T neutron fraction appears to impact saturation activity values, at least those resulting from neutron capture reactions. Thus both the D–D and the D–T neutron sources must be modeled. Another crucial parameter required by most of the unfolding codes is the input neutron energy spectrum. This input guess has to be rather close to the real spectrum to obtain meaningful output from these codes [22–24]. An extensive effort was investigated in unfolding neutron energy spectra for the IEs. The details of this effort will form the subject of another publication which will also include further improvements. Fig. 10 compares preliminary unfolded neutron energy spectra for IE 8 and 3, normalized to 1 D–T n cm^{-2} in the energy range from 13.5 to 15 MeV. As qualitatively expected, the spectrum is considerably softer for IE 3 than for IE 8.

6. Relevance of the measurements to ITER

The unfolded energy spectrum for IE 8 on TFTR can be compared with those expected for the first wall for ITER and measured in a prototypical USDOE–JAERI irradiation assembly (Fig. 11). Each spectrum has been normalized to 1 D–T n cm^{-2}. The neutron spectrum for ITER (ITER-FW) is for a first wall with a self-cooled Li–V blanket option, under extensive study at one time [25]. The spectrum for a water-cooled design is also available and shows a considerably higher fraction of low energy neutrons [25]. The neutron energy spectrum of the USDOE–JAERI program (US/J-FW) is for a location that is about 5 cm deep inside a lithium oxide region behind an SS first wall, with a coolant channel assembly of phase IIC [4]. One observes that although there are differences in the three spectra in practically the entire energy range, the spectral shapes are comparable. We have used the normalized spectra to calculate saturation activities for various dosimetric reactions using the activation cross-section library of DKR-ICF [26]. The calculated activities are shown in

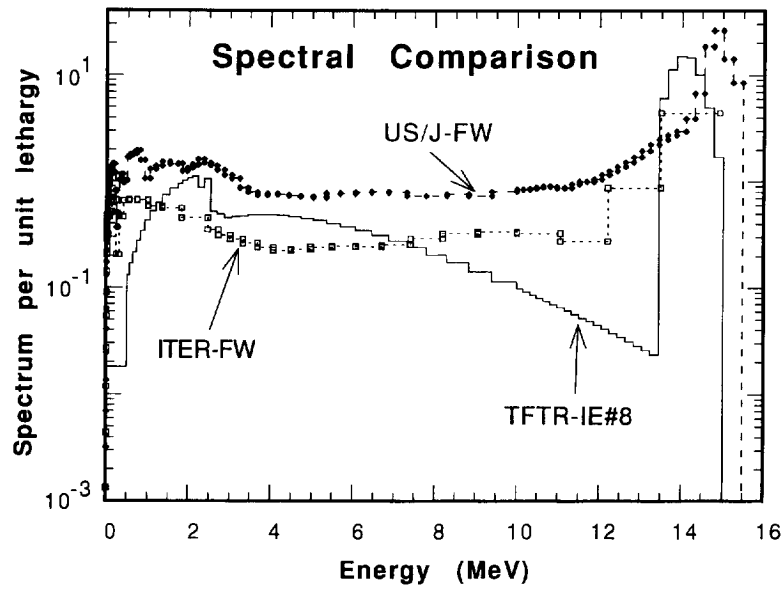

Fig. 11. Comparison of normalized spectra per unit lethargy for first wall of ITER (ITER-FW) (self-cooled Li–V blanket option), first-wall-kind spectrum for position B of USDOE–JAERI collaborative program (US/J-FW), and IE 8 of TFTR (TFTR-IE 8). Each spectrum is normalized such that there is 1 n cm^{-2} (say, 1 D–T n cm^{-2}) in the energy range 13.5–15 MeV.

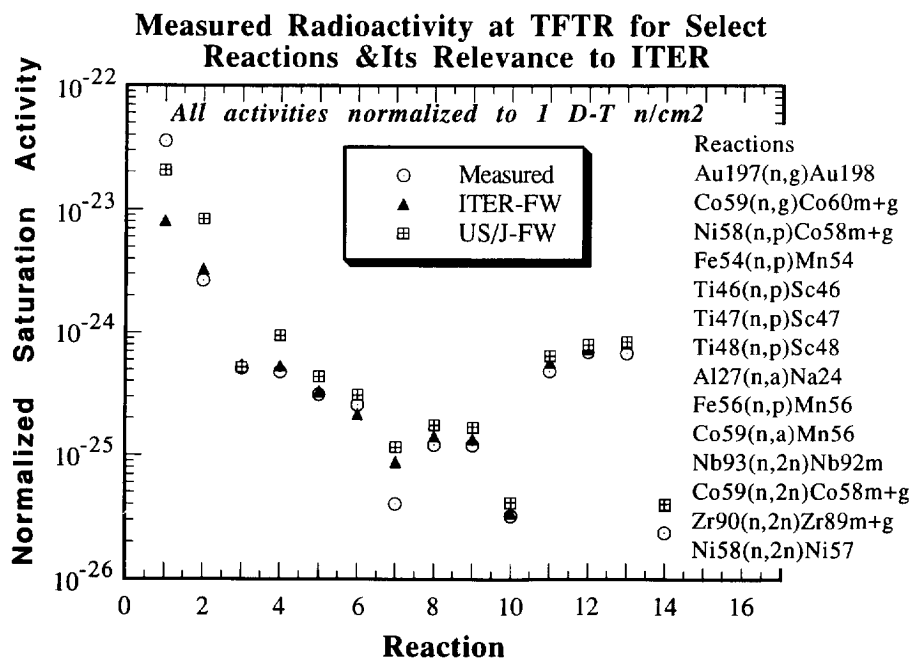

Fig. 12. Comparison of normalized, measured, saturation activities for ITER filrst wall of self-cooled Li–V option (ITER-FW), USDOE–JAERI collaborative program first wall like (US/J-FW), and TFTR IE 8. The normalization is done to 1 D–T n cm^{-2} for both calculated as well as measured saturation activity.

Fig. 12 together with the measured saturation activities on TFTR for IE 8, all normalized to 1 D–T n cm^{-2}. The calculated and the measured activities generally look remarkably comparable. Whatever differences exist are to be assigned to old activtion cross sections as well as differences in neutron energy spectra. Thus the measurements of radioactivity at the TFTR IEs provide a useful validation of ITER calculations.

7. Summary and conclusions

Extensive measurements of radioactivity induced by fusion neutrons in various materials of interest to ITER were carried out at TFTR. The measurements were done at IE inside and outside the vacuum vessel. Clear differences were observed in saturation activities for the three irradiation ends, especially for threshold reactions. Saturation activities of capture reactions showed an approximately 50% dependence on the D–T neutron fraction. The measured saturation activities for dosimetric reactions were unfolded to obtain the neutron energy spectra. A comparison of measured activities was then done to the calculations for an ITER first wall and a first-wall-type location of a USDOE–JAERI experimental assembly. In spite of differences for some reactions, the normalized, measured activities were found comparable with those for the ITER first wall.

Acknowledgments

We thank Dale Meade (PPPL) for encouraging this collaboration, and Ken Young (PPPL) for supporting it. Stjepko Sesnic (PPPL) helped operate the pneumatic system during some of the experiments. We also thank Greg Lemunyan (PPPL) and Richard Scarberry and Hank Alvestad (LANL) for technical support of the neutron activation system. This work was supported by US DOE Contracts W-7405-ENG-36, DE-AC02-76CH03073, and DE-FG03-86ER52123.

References

[1] A. Kumar and Y. Ikeda, On disagreement between measurements and calculations of D–T neutron driven induced radioactivity and nuclear heating, Proc. Int. Conf. on Nuclear Data for Science and Technology, Gatlinburg, TN, May 9–13, 1994, pp. 883–895.

[2] A. Kumar, M.A. Abdou, Y. Ikeda and C. Konno, Radioactivity and nuclear heating meaurements for fusion applications, Fusion Technol. 18 (1990) 872–876.

[3] A. Kumar, M.A. Abdou, Y. Ikeda and T. Nakamura, Analysis of induced activities measurements related to decay-heat in phase IIC experimental assembly: USDOE/JAERI collaborative program on fusion neutronics experiments, Fusion Technol. 19 (1991) 1909–1918.

[4] A. Kumar, Y. Ikeda, M.A. Abdou, M.Z. Youssef, C. Konno, K. Kosako, Y. Oyama, T. Nakamura and H. Maekawa, Induced radioactivity measurements in fusion neutron environment: joint report of USDOE/JAERI collaborative program on fusion neutronics, Reps. UCLA-ENG-91-32/UCLA-FNT-53 and JAERI-M-93-018, February 1993.

[5] A. Kumar, M.A. Abdou, M.Z. Youssef, Y. Ikeda et al., Measurements of decay radioactivity of long-lived isotopes, Fusion Technol. 21 (1992) 2180–2189.

[6] R.T. Santoro, J.M. Barnes, R.G. Alsmiller, Jr., et al., Comparisons of calculated and measured spectral distributions of neutrons from a 14-MeV neutron source inside the Tokamak Fusion Test Reactor, Fusion Technol. 11 (1987) 420–428.

[7] J.K. Dickens, J.W. McConnell, K.M. Chase et al., Measurements of the neutron and gamma-ray fluences in the TFTR test cell due to a point source simulating D–T fusion plasma neutron production, Fusion Technol. 12 (1987) 270–280.

[8] H.W. Kugel, C.W. Barnes, J. Gilbert et al., Measurements of TFTR radiation shielding during high power D–D operations, Fusion Technol. 19 (1991) 1989–1995.

[9] F. Hajnal, N. Azziz, K. Decker et al., Measurement of the neutron radiation fields at the Princeton Tokamak Fusion Test Reactor (TFTR), Final Rep., 1991.

[10] H.W. Kugel et al., TFTR radiation contour and shielding efficiency measurements during D–D operations, Fusion Technol. 26 (1994) 963–972.

[11] J.D. Strachan et al., Fusion power production from TFTR plasmas fueled with deuterium and tritium, Phys. Rev. Lett. 72 (1994) 3526.

[12] A. Kumar, M.A. Abdou and H.W. Kugel, Characterization of TFTR shielding penetrations of ITER relevance in D–T neutron field, Fusion Eng. Des. 28 (1995).

[13] E.B. Nieschmidt, Analysis programs and standardization of the neutron activation system at TFTR, Rev. Sci. Instrum. 57 (1986) 1757–1759.

[14] E.B. Nieschmidt, T. Saito, C.W. Barnes et al., Calibration of the TFTR neutron activation systems, Rev. Sci. Instrum. 59 (1988) 1715–1717.

[15] C.W. Barnes, E.B. Nieschmidt, A.G.A. Huibers et al., Operation and cross calibration of the activation foil system on TFTR, Rev. Sci. Instrum. 61 (1990) 3190–3192.

[16] C.W. Barnes, A.R. Larson, G. Lemunyan and M.J. Loughlin, Measurements of DT and DD neutron yields by neutron activation on the Tokamak Fusion Test Reactor, Rev. Sci. Instrum. (1994) to be published.

[17] C.W. Barnes and A. Larson, Review of MCNP neutron activation calculations for the TFTR re-entrant irradiation end, and uncertainty analysis for neutron yields, LANL Memo, October 27, 1993, to be submitted to Fusion Technol. (1994).
[18] E. Browne and R.B. Firestone, in V.S. Shirley (ed.), Table of Radioactive Isotopes, Wiley–Interscience, New York, 1986.
[19] C.M. Lederer and V.S. Shirley, Table of Isotopes, New York, 7th edn., 1978.
[20] E. Storm and H.I. Israel, Photon cross-sections from 1 keV to 100 MeV for elements $Z = 1$ to $Z = 100$, Nucl. Data Tables A, 7 (1970) 565–581.
[21] J.F. Briesmeister (ed.), MCNP – A general Monte Carlo code for neutron and photon transport: version 3A, Rep. LA-7396-M, rev. 2, September 1988.
[22] F.G. Perey, STAY'SL: least squares dosimetry unfolding code system, RSIC computer code collection PSR-113, March 1984.
[23] A. Kumar, Source normalization in least-squares dosimetry unfolding, Trans. Am. Nucl. Soc. 47 (1984) 155.
[24] F.B.K. Kam, SAND II: neutron flux spectra determination by multiple foil activation—iterative method, RSIC computer code collection CCC-112 June 1975.
[25] H.Y. Khater, personal communications to A. Kumar, March 23, 1994, and June 1, 1994.
[26] D.L. Henderson and O. Yasar, A radioactivity and dose rate calculation code package, Vols. 1 and 2, RSIC computer code collection, CCC-323, April 1987.